Earthquake Engineering & Structural Dynamics
The Journal of the International Association for Earthquake Engineering

EARTHQUAKE ENGINEERING & STRUCTURAL DYNAMICS
Earthquake Engng Struct. Dyn. 2014; **43**:1173–1191
Published online 26 November 2013 in Wiley Online Library (wileyonlinelibrary.com). DOI: 10.1002/eqe.2392

Enhancing resilience of highway bridges through seismic retrofit

Ashok Venkittaraman[1] and Swagata Banerjee[2,*,†]

[1]*Technip North America, Houston, TX 77079, USA*
[2]*Department of Civil and Environmental Engineering, The Pennsylvania State University, University Park, PA 16802, USA*

SUMMARY

The present study evaluates seismic resilience of highway bridges that are important components of highway transportation systems. To mitigate losses incurred from bridge damage during seismic events, bridge retrofit strategies are selected such that the retrofit not only enhances bridge seismic performance but also improves resilience of the system consisting of these bridges. To obtain results specific to a bridge, a reinforced concrete bridge in the Los Angeles region is analyzed. This bridge was severely damaged during the Northridge earthquake because of shear failure of one bridge pier. Seismic vulnerability model of the bridge is developed through finite element analysis under a suite of time histories that represent regional seismic hazard. Obtained bridge vulnerability model is combined with appropriate loss and recovery models to calculate seismic resilience of the bridge. Impact of retrofit on seismic resilience is observed by applying suitable retrofit strategy to the bridge assuming its undamaged condition prior to the Northridge event. Difference in resilience observed before and after bridge retrofit signified the effectiveness of seismic retrofit. The applied retrofit technique is also found to be cost-effective through a cost-benefit analysis. First order second moment reliability analysis is performed, and a tornado diagram is developed to identify major uncertain input parameters to which seismic resilience is most sensitive. Statistical analysis of resilience obtained through random sampling of major uncertain input parameters revealed that the uncertain nature of seismic resilience can be characterized with a normal distribution, the standard deviation of which represents the uncertainty in seismic resilience. Copyright © 2013 John Wiley & Sons, Ltd.

Received 12 May 2013; Revised 17 October 2013; Accepted 25 October 2013

KEY WORDS: resilience; highway bridges; seismic fragility; parameter sensitivity; random sampling; benefit-cost analysis

1. INTRODUCTION

A natural disaster is the consequence of an extreme natural hazard such as earthquake, flood, hurricane, tornado, and landslide. It leads to economic, human, and/or environmental losses to a society. The resulting loss depends on the resistance of the affected population to survive against the disastrous event, called its resilience. Disaster resilience of a civil infrastructure system is defined in literature as a function that indicates the capability of the system to sustain a level of functionality over a period decided by owners or the society.

Bridges are significant component of highway transportation systems that serve as a key mode of ground transportation and sometimes act as an important feeder system to other modes of transportation such as railroad systems, port facilities, and air travel. Damage of highway bridges due to extreme events may cause severe disruption to the normal functionality of highway transportation systems and may further impact on the performance of other modes of transport. Bridge damage not only causes direct economic losses due to postevent bridge repair and restoration

*Correspondence to: Swagata Banerjee, Department of Civil and Environmental Engineering, The Pennsylvania State University, University Park, PA 16802, USA.
†E-mail: swagata@engr.psu.edu

but also produces indirect losses arising from network downtime, traffic delay, and business interruptions. Failure of large numbers of highway bridges in California during the 1971 San Fernando, 1989 Loma Prieta, and 1994 Northridge earthquakes has severely disrupted the normal functionality of regional highway transportation systems and caused sudden and undesired changes in technical, organizational, societal, and economic conditions of communities served by these systems. Prevention is better than cure—this simple yet powerful adage becomes of profound importance when such a disaster condition is thought of. Along this line, 'recovery' and 'resilience' have become key points in dealing with extreme events, if not to prevent completely, but to minimize their negative consequences and to maximize disaster resilience of highway transportation systems.

Seismic retrofitting of highway bridges is one of the most common approaches undertaken by state Departments of Transportation (state DOTs) and bridge owners to enhance system performance of bridges during seismic events. Types of seismic retrofit strategies applied to a bridge depend on various factors including bridge attributes, configurations, accessibility, and demand from seismic hazard. Common seismic retrofit techniques for bridges include lateral confinement of bridge piers using steel or composite jackets, installation of restrainers at abutments and expansion joints, seismic isolation through bearings, and installation of bigger foundations [1–4]. While all these bridge retrofit techniques may be effective in mitigating seismic risk of bridges, adequacy of their application and effectiveness may greatly depend on enhanced seismic functionality of highway network because of retrofit, reduction in postearthquake losses, and benefit to cost ratio of bridge retrofitting. Hence, the basis for selecting bridge retrofit technique should include expected postevent losses and cost incurred from seismic retrofit in addition to the enhancement in bridge performance and network functionality. In this relation, calculation of resilience is identified as a meaningful way to express loss and recovery of system functionality after a natural disaster [5–15]. Seismic resilience of a highway bridge can be represented as an integrated measure of bridge seismic performance, expected losses, and recovery after the occurrence of seismic events. Therefore, calculation of bridge resilience before and after the application of a retrofit strategy will not only indicate the effectiveness of this strategy in improving bridge seismic performance but also exhibit the impact of retrofit on system functionality under regional seismic hazard.

This present study evaluates effectiveness of retrofit techniques to enhance seismic resilience of highway bridges. A reinforced concrete bridge in the La Cienega-Venice Boulevard sector of Santa Monica (I-10) freeway in Los Angeles, California is selected as a test-bed bridge. This freeway runs across eight states from Florida to the Pacific. In 1993, this freeway was reported to be the world's busiest freeway carrying an approximate average daily traffic of 261,000 [16]. During the 1994 Northridge earthquake, the test-bed bridge was severely damaged primarily because of shear failure of one of the bridge piers. Postevent reconnaissance indicated that the failure was initiated from inadequate lateral confinement of pre-1971 designed bridge piers. Due to this, vertical load carrying capacity of the bridge reduced significantly during the seismic event resulting in crushing of core concrete and buckling of longitudinal rebars of bridge piers [17]. Seismic vulnerability of the predamaged bridge is assessed through finite element (FE) analysis of the bridge under a suite of time histories that represent seismic hazard at the bridge site. Seismic resilience of the as-built bridge is calculated using appropriate loss and recovery models. To observe the effectiveness of bridge retrofit in enhancing seismic resilience, bridge piers are retrofitted with steel jackets assuming the undamaged condition of the bridge prior to the Northridge event. Seismic vulnerability of the retrofitted bridge is estimated to calculate seismic resilience after retrofitting. Difference in seismic resilience before and after retrofit is considered to be a signature representing the adequacy and effectiveness of applied retrofit technique. Cost-benefit study is performed assuming 30 to 50 year service life of the retrofitted bridge to evaluate the cost-effectiveness of applied seismic retrofit technique.

First order second moment (FOSM) reliability analysis is performed to identify major uncertain input parameters to which seismic resilience of the original un-retrofitted bridge estimated for the Northridge earthquake is most sensitive. For this, parameter uncertainties associated with bridge vulnerability analysis and resilience estimation modules are considered. A tornado diagram is developed to further support the observations made from FOSM analysis regarding the hierarchy of

DOI: 10.1002/eqe

uncertain input parameters. To characterize the uncertain nature of seismic resilience, statistical analysis of resilience obtained through random sampling of major uncertain input parameters is performed. Though seismic hazard is discussed in this paper, the described approach of selecting the most suitable retrofit strategy can be extended to other types of natural hazards and structural type.

2. SEISMIC RESILIENCE

Past studies have defined and calculated resilience of various lifeline systems such as acute care hospitals, water supply systems, power transmission systems, and transportation systems [5–15]. In general, resilience is defined in these studies as a dimensionless quantity representing the rapidity of the system to revive from a damaged condition to the predamaged functionality level. Loss due to a natural event and postevent performance recovery of a system are the two major components to quantify disaster resilience of a civil infrastructure system. For a single seismic event, resilience can be expressed as [12]

$$R = \int_{t_{0E}}^{t_{0E}+T_{LC}} \frac{Q(t)}{T_{LC}} \mathrm{d}t \tag{1}$$

where t_{0E} represents the time when the extreme event E occurs and T_{LC} is a controlled time set to evaluate resilience. $Q(t)$ represents system functionality, which can be expressed as a dimensionless function of time t. Figure 1(a) schematically represents system functionality before and just after a seismic event and during the postevent recovery process. Therefore, resilience is the area of this functionality curve between t_{0E} and $t_{0E}+T_{LC}$ averaged over T_{LC}. The analytical expression of $Q(t)$, given in the following equation, constitutes a loss function and a recovery function of system performance during the period of system interruption because of the extreme event [18].

$$Q(t) = 1 - [L(I, T_{RE}) \times \{H(t - t_{0E}) - H(t - (t_{0E} + T_{RE}))\} \times frec(t, t_{0E}, T_{RE})] \tag{2}$$

Here, $L(I,T_{RE})$ is the loss function, f_{rec} is the recovery function, I is seismic intensity, and T_{RE} is the recovery time for event E. Figure 1 also schematically represents three recovery functions, namely, linear, trigonometric, and negative exponential functions. $H()$ is the Heaviside step function; this discontinuous function takes value equal to either one or zero based on positive and negative arguments. Calculation of loss requires the information on system vulnerability under natural disaster. As can be seen from Equation (2), $Q(t) = 1.0$ in case of no loss and $0 < Q(t) < 1.0$ when there is loss due to seismic damage. Therefore, resilience is measured as a percentage of functionality. For a fully serviceable system without any loss in functionality after an extreme event, $R = 100\%$. Otherwise, $0 < R < 100\%$ based on the severity of damage and drop of system functionality because of seismic activity.

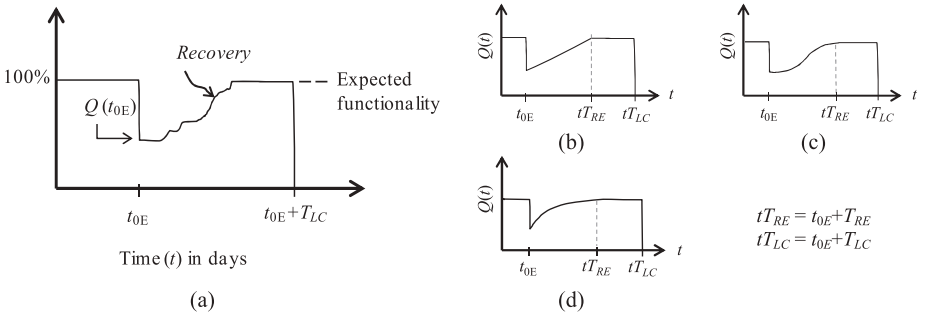

Figure 1. Schematic representation of disaster resilience and postevent recovery functions: (a) functionality curve, (b) linear recovery function, (c) trigonometric recovery function, and (d) negative exponential recovery function.

DOI: 10.1002/eqe

2.1. Vulnerability of a system or system component

For highway transportation systems, bridges are generally considered as the most seismically vulnerable components. The present study measures bridge vulnerability in the form of fragility curves. Fragility curves represent the probability of exceeding in a bridge damage state under certain intensity of ground motions such as peak ground acceleration or PGA [19, 20]. Two-parameter lognormal distributions are generally used to develop fragility curves. The analytical expression of a fragility curve is given as

$$F\left(\mathrm{PGA}_j, c_k, \zeta_k\right) = \Phi\left[\frac{\ln\left(\mathrm{PGA}_j/c_k\right)}{\zeta_k}\right] \tag{3}$$

where PGA_j represents PGA of a ground motion j and k represents bridge damage states such as minor, moderate, major damage, and complete collapse. The two parameters c_k (median value) and ζ_k (log-standard deviation) are fragility parameters for a damage state k. These parameters can be estimated by maximizing the likelihood function L given as follows.

$$L = \prod_j \left[F\left(\mathrm{PGA}_j, c_k, \zeta_k\right)\right]^{r_j}\left[1 - F\left(\mathrm{PGA_j}, c_k, \zeta_k\right)\right]^{1-r_j} \tag{4}$$

Here, $r_j = 0$ or 1 depending on whether or not the bridge sustains the damage state k under the j^{th} ground motion. Other intensity measures such as peak ground velocity, spectral acceleration, spectral velocity, and spectral intensity can also be used to represent seismic intensity. However, the use of any of the above intensity measures in the development of seismic fragility curves provides no additional advantage over the use of PGA [21].

2.2. Loss function

The loss function incorporates all direct and indirect losses from a postevent degraded system over the period of system restoration. The direct loss for a bridge seismic damage arises because of bridge restoration after the seismic event. It includes the cost associated with postevent repair and rehabilitation of damaged bridges or bridge components. Hence, direct loss due to a seismic event can be calculated by multiplying the occurrence probability of the event and failure probability of a system (or system component) under this event [22, 23]. For a bridge, direct economic loss (C_{rE}) resulted from an event E can be evaluated in terms of a dimensionless cost term L_D that represents the ratio of restoration cost C_{rE} to replacement cost C as

$$L_D = \frac{C_{rE}}{C} = \sum_k P_E(DS = k) \times r_k \tag{5}$$

where k represents the damage states of the bridge, P_E $(DS = k)$ is the probability of bridge failure at damage state k during the seismic event E, and r_k is the damage ratio corresponding to damage state k. Values of P_E $(DS = k)$ and r_k can be obtained, respectively, from bridge fragility curves developed for various damage states and HAZUS [24]. Replacement cost C can be evaluated by multiplying bridge deck area with the unit area replacement cost [22].

Indirect loss (L_{ID}) arises because of the disrupted functionality of the system after an event. For highway transportation systems, indirect losses consist of rental, relocation, business interruptions, traffic delay, loss of opportunity, losses in revenue, and so on. In addition, casualty losses may also be included in the indirect loss model to calculate resilience of critical care facilities such as hospitals [12]. Indirect losses are time dependent. These losses are maximum immediately after the extreme event and gradually reduce as bridge restoration takes place. Past studies on highway bridges have taken indirect loss to be 5–20 times greater than the direct loss [25]. More specific value of indirect to direct loss ratio can be calculated if information on traffic flow in a highway network before and after an earthquake can be obtained and dynamic equilibrium using network

DOI: 10.1002/eqe

capacity and traffic demand can be established [22]. Such as comprehensive traffic analysis is beyond the scope of the present study. Hence, an expected value for indirect to direct loss ratio of 13 is assumed in this study for each bridge damage state. A similar approach has been adopted in Denneman [25]. A sensitivity study presented later in this paper investigated the impact of this ratio on seismic resilience.

2.3. *Recovery function*

The recovery function (f_{rec}) describes a path following that postevent restoration of bridges is expected to take place. Development of an appropriate mathematical model for the recovery function involves extreme difficulty because of the dependence of postevent bridge recovery process on several factors including the availability of fund. Cimellaro [15] suggested the generation of empirical or analytical recovery functions based on real-life data or on the type of analysis. For analytical recovery functions, five different recovery functions are proposed that are further grouped under short-term and long-term recovery models. Among these, the long-term recovery models are of interest here as the present study includes the postevent recovery phase within the framework of resilience estimation. Long-term recovery models included linear, negative exponential, and trigonometric recovery functions. A linear postevent bridge recovery process with a probabilistic distribution of postevent recovery time is also proposed by Zhou *et al*. [22] on the basis of bridge recovery processes observed in real-time after severe earthquakes in past. These previous studies used same recovery pattern (i.e., either linear or trigonometric or exponential) irrespective of seismic damage states of structural components. Decò *et al*. [14] proposed to use different recovery patterns for different seismic damage states of bridges because bridges with different seismic damage states may have different levels of accessibility after the seismic event. A variety of postevent bridge restoration patterns (such as positive and negative exponential and stepwise) are assigned to different bridge damage states on the basis of subjective judgments.

Time required to complete a bridge restoration is not a unique quantity; it greatly depends on the severity of bridge damage because of the extreme event. Zhou *et al*. [22] considered that the time required to complete a bridge restoration is a random variable uniformly distributed between the maximum and minimum required times to complete the restoration job. In the seismic loss estimation manual [26], recovery times for different seismic damage states of highway bridges are modeled with normal distribution functions, distribution parameters (mean and standard deviation) of which are given in Table I. These distributions were originally developed based on earthquake damage evaluation data acquired for California [27]. As can be seen from this table, high standard deviations of postevent restoration times were observed, especially at lower bridge damage states. This is because of limited available data on the time required for post-seismic bridge recovery. These probabilistic models can be updated if more data from regional earthquakes become available. As the test-bed bridge is located in California, the recovery times given in Table I are used in the present study.

3. MODELING AND VALIDATION OF THE TEST-BED BRIDGE

The test-bed bridge considered in this study connects I-10 freeway and the La Cienega Boulevard in California. It is a multispan reinforced concrete bridge as shown Figure 2 (schematic). Bridge superstructure is composed of 1.58-m deep and 2.06-m wide multicell hollow box girders. Cross-sectional and material properties of bridge girder are obtained from Broderick and Elnashai [28] and

Table I. Mean and standard deviation of post-seismic restoration times for highway bridges [26].

Bridge damage state (days)	Slight/minor	Moderate	Extensive	Complete
Mean	0.6	2.5	75	230
Standard deviation	0.6	2.7	42	110

DOI: 10.1002/eqe

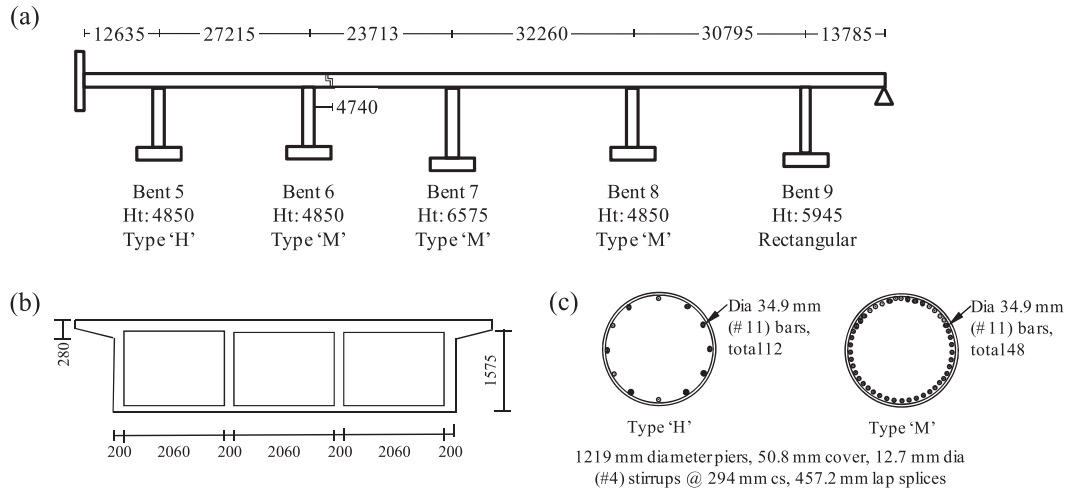

Figure 2. (a) The test-bed bridge (schematic), (b) cross-section of bridge girder, and (c) cross sections of type 'H' and 'M' piers (all units are in mm).

Lee and Elnashai [29]. The bridge is supported on six 1.219-m diameter circular piers at four bent locations. Bent 5 is a multicolumn bent with three identical piers. Bents 6 to 8 each has single pier with the same diameter as of the piers in bent 5. Based on reinforcement used, these piers have either type 'H' (in bent 5) or type 'M' (in bents 6 to 8) cross sections (Figure 2). Bent 9 has a rectangular wall section. All pier–girder connections are monolithic. Specific properties of these bents are discussed later in this paper. The bridge has an in-span expansion joint just after bent 6.

Broderick and Elnashai [28] analyzed the nonlinear response of the bridge under the Northridge earthquake ground motions and made a qualitative comparison between analytical bridge response with that observed during the earthquake. As the bridge was a part of freeway system, it was difficult to numerically simulate the accurate boundary condition of the bridge. Broderick and Elnashai [28] developed four FE bridge models by changing boundary conditions. Effectiveness of these four models was judged by comparing the numerical response of the bridge with that observed during the Northridge earthquake. This comparison showed that the consideration of fixed boundary on freeway side (west side) and hinged boundary (i.e., moment release) on the east side of the bridge provided the closest match between numerical and observed bridge response. Thus, the comparison helped in establishing a realistic numerical model for the bridge. To pursue the present study, results presented in Broderick and Elnashai [28] are used as baseline to validate the FE model of the bridge developed as a part of the present study. Consistency is maintained in assigning boundary conditions and material properties of various bridge components for model valuation (Figure 2).

3.1. Modeling of bridge components

Finite element model of the bridge is developed using SAP2000 [30]. Modeling of various bridge components and their geometric and material properties are discussed next.

3.1.1. Bridge girder. A 140.4-m long bridge girder is modeled using linear elastic beam–column elements as this component of the bridge is expected to respond within the elastic range during seismic excitation. These beam–column elements are aligned along the center line of the bridge deck. To obtain properties of beam–column elements, cross section of bridge girder is modeled in STAAD [31], and obtained properties are used in SAP2000 as input.

3.1.2. Bridge piers. During seismic excitation, the maximum bending moment generates at pier ends. This often leads to the formation of plastic hinges at these locations when the generated moment exceeds the plastic moment capacity of these sections. To model such nonlinear behavior at bridge pier ends, nonlinear rotational springs are introduced in bridge models at the top and bottom of each

DOI: 10.1002/eqe

pier. Rigid elements are assigned at pier ends (i.e., at pier–girder and pier–foundation connections). This ensures rigid connectivity at pier–girder connections of monolithic concrete bridges. The cap beam for the three piers in bent 5 is modeled as a rigid link. Figure 3 shows the computed (actual) and bilinear moment–rotation envelopes of bridge piers that are developed through the moment–curvature analysis described in Priestley *et al*. [32]. In these figures, M_y and M_u represent the yield and ultimate moment carrying capacities of the pier cross sections, respectively, and θ_y and θ_u are corresponding rotations. k_{elastic} represents the initial elastic stiffness of the member, and α is the post-yield stiffness ratio. Axial load levels on these piers vary from pier to pier because of which moment–rotation relations of piers in bents 6, 7, and 8 are different although they have the same cross-sectional and material properties.

3.1.3. In-span expansion joint. At in-span expansion joint, the bridge is modeled such that the two ends of the expansion joint can move independently in the longitudinal direction and rotate in the longitudinal plane, while they have no relative vertical movement. During out-of-plane motion, they are assumed to have a pin connection. The opening and closure of an expansion joint during bridge movement are modeled by assigning hook and gap elements, respectively [19]. The hook element represents the effect of restrainer at expansion joint and controls relative displacement (excessive separation) between two adjacent girders at the expansion joint. A nonlinear link element with an initial slack of 25.4 mm is used as a hook element. Force develops in this element when the outward relative displacement of adjacent bridge decks is more than initial slack. A nonlinear gap element with an initial gap of 12.7 mm and linear elastic stiffness of 223.3 MN/m (calculated according to [17]) for longitudinal translation are assigned. Hence, the gap element becomes active only when the relative inward displacement of adjacent bridge decks in the longitudinal direction of the bridge exceeds the initially provided gap width of 12.7 mm.

3.1.4. Foundation. The bridge was located on the site of an old river bed [28]. Stiffness of bridge foundation should be calculated according to the local site profile. For the purpose of model validation, fixed condition is assumed at all pier bottoms to be consistent with the analysis performed by Broderick and Elnashai [28]. After validated, appropriate foundation models are assigned to realistically capture soil–foundation interactions at bridge foundations.

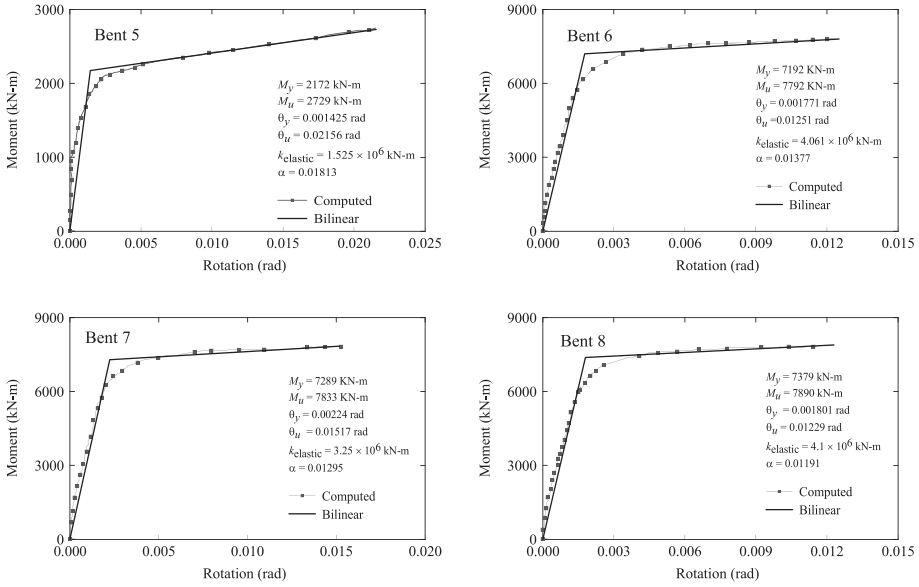

Figure 3. Moment–rotation diagrams of piers in bent 5 to bent 8.

DOI: 10.1002/eqe

3.2. Northridge earthquake ground motions records

For model validation, the bridge is analyzed for the two horizontal orthogonal components of the Northridge earthquake recorded at the City Hall station (in Santa Monica), which is approximately 10 km away from the bridge site. This is the nearest recording station from the bridge site amongst several others located in this region. PGAs of these two components were recorded to be 0.370 and 0.883 g, propagated along the longitudinal, and transverse directions of the bridge, respectively. Figure 4 shows complete time histories of the recorded motion components that are obtained from PEER strong motion database.

3.3. Bridge response under the Northridge earthquake and model validation

Fundamental periods and mode shapes of the bridge at first five modes are presented in Table II as obtained from the present study and Broderick and Elnashai [28]. This table depicts that obtained dynamic properties of the bridge from the present study are in well agreement with that calculated in a previous research. Table III shows shear capacities of bridge piers in bents 6, 7, and 8 calculated following Priestley *et al*. [32]. Shear demands of these piers are represented by shear forces developed during the Northridge earthquake. These shear demands are obtained from nonlinear time history analysis of the bridge when two orthogonal components of the Northridge earthquake are applied simultaneously. Comparison of shear capacity with demand shows that pier in bent 6 fails in shear as the demand exceeds capacity at this location. The same phenomenon is also observed during the Northridge earthquake. A similar observation is also made by Broderick and Elnashai [28]. Hence, these comparisons confirm the validity of the FE model of the test-bed bridge developed for this study.

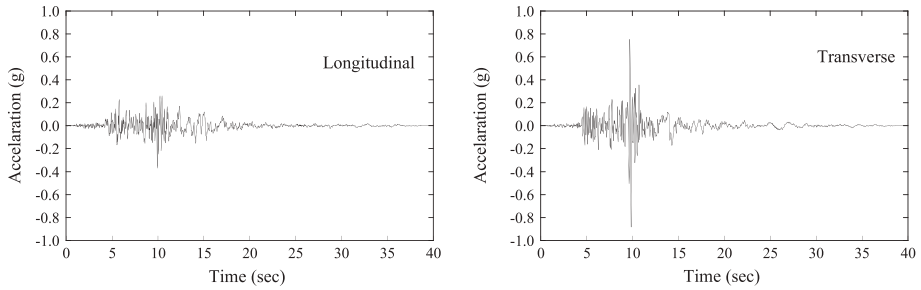

Figure 4. Northridge earthquake ground motion components recorded at the City Hall station.

Table II. Comparison of modal shapes and fundamental periods of the bridge.

	From the present study		From Broderick and Elnashai [28]	
Modes	Period	Mode shape	Period	Mode shape
1	0.44	Transverse	0.46	Transverse
2	0.29	Transverse	0.28	Transverse
3	0.24	Deck	0.20	Deck
4	0.20	Deck	0.16	Deck
5	0.18	Deck	0.16	Deck

Table III. Shear capacities and shear demand at bridge piers.

Location of bridge pier	Shear capacity (KN)	Shear demand (KN)	Conclusion
Bent 6	2537	2540	Pier in bent 6 failed in shear
Bent 7	2353	2063	
Bent 8	2715	2362	

DOI: 10.1002/eqe

4. SEISMIC RESILIENCE OF THE BRIDGE

Broderick and Elnashai [28] used fixed conditions at bridge pier bases. The same condition is considered in the initial FE model of the test-bed bridge for the validation purpose. Post-validation, boundary conditions at pier bases are revised to include the effect of foundation–soil interaction on dynamic response of the bridge. From literature, it is found that type 'M' and 'H' piers of the bridge were supported on groups of 14 and 12 piles, respectively [28]. Each pile had 0.4 m diameter. Consequently, translational foundation springs are assigned at pier bottoms in the longitudinal and transverse directions of the bridge. Spring constants in lateral direction are calculated considering 7 kN/mm lateral stiffness of each pile [33, 34]. Thus, lateral foundation stiffness for type 'M' and 'H' piles is calculated to be 98 and 84 kN/mm, respectively. Foundation joints are restrained in the vertical direction, and rotational degrees of freedom at these joints about all directions are constrained.

4.1. Bridge fragility curves

To develop fragility curves, time history analyses of the bridge are performed under 60 ground motions that were originally generated by the Federal Emergency Management Agency for the Los Angeles region in California.[1] These ground motions include both recorded and synthetic motions and are categorized into three sets having annual exceedance probabilities of 2%, 10%, and 50% in 50 years. Each set has 20 ground motions. The wide range of seismic hazard covered through these motions is preferable for seismic fragility analysis of the bridge.

During the Northridge earthquake, a major horizontal ground motion component propagated along the transverse direction of the bridge resulting in shear failure of pier in bent 6 in this direction. Hence, the test-bed bridge is most vulnerable in the transverse direction. To be consistent with the actual damage of the bridge, seismic fragility analysis is performed by applying ground motions in the transverse direction of the bridge. Bridge seismic damage is characterized through shear and flexural failures of bridge piers. These two failure modes are assumed to govern the global failure of the bridge. Other possible seismic bridge failure modes such as unseating of bridge girders and failure at expansion joint are assumed to be non-governing failure modes. In general, shear failure of a bridge pier is brittle in nature and sometimes causes irreversible damage to bridges. Hence, such a mode of failure is considered here as an ultimate damage (i.e., complete collapse) of the bridge. For flexural damage of bridge piers, HAZUS [24] provided five different bridge damage states namely no, minor (or slight), moderate, major (or extensive) damage, and complete collapse. Among these, the complete collapse state is the ultimate damage state of the bridge, and others are named according to the severity of bridge seismic damage without complete collapse.

To generate fragility curves of the bridge, shear and flexural damage of the bridge are defined in a quantitative manner. Seismic damage states are ranked with $k = 1$ to 4 in which $k = 1$ represents minor damage and $k = 4$ represents complete collapse. If shear failure occurs because of the j^{th} ground motion, the bridge is considered to have damage condition $r_j = 1$ at damage state $k = 4$ (Equation (4)). For flexural damage, bridge damage condition ($r_j = 0$ or 1) at a particular damage state is defined on the basis of rotational ductility of bridge piers. By definition, rotational ductility (μ_θ) is the ratio of rotation (θ) of bridge piers to the yield rotation (θ_y) measured at the same location. Thus, rotational ductility of all piers at yield is equal to 1.0 ($=\theta_y/\theta_y$), whereas the same for the ultimate state ($=\theta_u/\theta_y$; θ_u is ultimate rotation of bridge piers, Figure 3) will vary from pier to pier. During time history analyses of the bridge under 60 motions, rotational time histories are recorded at both top and bottom of all bridge piers where plastic hinges are likely to appear. Rotational ductility for each pier is obtained by dividing maximum rotations from rotational time histories with yield rotations of corresponding locations that are obtainable from moment–rotation plots shown in Figure 3. These rotational ductility values are considered as a signature representing the flexural response of the bridge under seismic motions.

To define damage condition of the bridge at each damage state due to flexure under 60 ground motions, rational ductility values are compared with threshold limits. These threshold limits for each

[1] http://nisee.berkeley.edu/data/strong_motion/sacsteel/ground_motions.html

DOI: 10.1002/eqe

bridge damage state are shown in Table IV. The bridge was constructed in 1964, so it is reasonable to assume that bridge piers were not properly designed to carry lateral loading from seismic events. The deficiency of lateral confinement in bridge piers was also evident from the post-Northridge reconnaissance report [17]. Due to this reason, threshold limits of rotational ductility for various seismic damage states of the bridge are calculated on the basis of drift limits of non-seismically designed bridge piers recommended in HAZUS [24]. Table IV shows the non-seismic drift limit ratios obtained from HAZUS [24] for bridge seismic damage state and corresponding threshold rotational ductilities of piers in bents 6, 7, and 8. Note that rotational ductility values of the bridge at no damage and complete collapse state are taken to be equal to the yield and ultimate rotational ductility of bridge piers, respectively. As threshold rotational ductility at ultimate state varies for pier to pier, the threshold values for intermediate damage states (i.e., minor, moderate, and major) also vary accordingly. Piers in bent 5 are excluded from this table. Piers in this multicolumn bent have low probability of forming plastic hinges compared to other single-column bents of the bridge. Also, shear forces developed in piers of bent 5 were low relative to their shear capacities. Hence, bent 5 is excluded from shear comparisons as well.

For each ground motion, damage condition of the test-bed bridge due to flexure is assigned by comparing rotational ductility values of bridge piers with corresponding threshold limits. For combined shear and flexural damage of the bridge under 60 motions, seismic fragility curves are developed at the minor, moderate, major damage, and complete collapse states (Figure 5). HAZUS [24] suggested an uncertainty factor for seismic demand to be equal to 0.5 based on the studies performed by Pekcan [35]. Following this, ζ_k is taken here as 0.5 for all damage states. This common ζ_k for all damage states restricts the intersection of any two fragility curves [36]. Median values for all damage states are reported within the figure. Note that higher median value indicates less probability of bridge damage in a damage state. These fragility curves indicates that the test-bed bridge has 100%, 99.7%, 95.3%, and 93.5% failure probabilities, respectively, in minor, moderate, major damage, and complete collapse states due to the transverse component of the Northridge

Table IV. Drift ratios and threshold values rotation ductility.

Damage states	Non-seismic drift ratio [24]	Threshold rotation ductility of bridge piers		
		Bent 6	Bent 7	Bent 8
No damage	0.002	1.00	1.00	1.00
Minor	0.005	1.37	1.36	1.36
Moderate	0.01	2.01	1.96	1.97
Major	0.02	3.28	3.16	3.18
Collapse	0.05	7.06	6.77	6.82

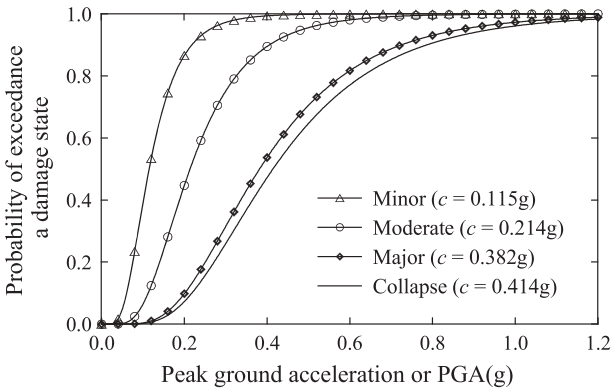

Figure 5. Seismic fragility curves of the test-bed bridge at four damage states.

DOI: 10.1002/eqe

earthquake (with PGA of 0.883 g). These high probabilities of failure indicate extensive damage of the bridge because of the Northridge earthquake. Thus, the fragility curves can appropriately simulate the seismic vulnerability of the bridge.

4.2. Direct and indirect losses due to the Northridge earthquake

The direct loss due to bridge damage during the Northridge earthquake is calculated following Equation (5). Damage ratios (r_k) at minor, moderate, major, and complete collapse states of the bridge are, respectively, 0.03, 0.08, 0.25, and 2/span number [24]. An overall cost ratio of 0.96 is obtained because of direct and indirect losses from the Northridge earthquake. A sensitivity study is performed the toward end of this paper by taking various ratios of indirect to direct losses.

4.3. Postevent seismic recovery

To observe the influence of different recovery models on seismic resilience of the bridge, three recovery models, linear, negative exponential, and trigonometric [12, 15], are used in this study in the absence of any precise, case-specific, and real-data-based recovery model for highway bridges. Table I provides the time required for complete recovery T_{RE} at various seismic damage states of the bridge.

4.4. Seismic resilience

Seismic resilience of the bridge due to the Northridge earthquake is calculated using Equations (1) and (2). Information on bridge seismic vulnerability as obtained from fragility curves (Figure 5) is combined with postevent loss and recovery functions. Percentage values of bridge seismic resilience are calculated to be 57.47%, 99.92%, and 57.69%, respectively, when linear, negative exponential, and trigonometric recovery functions are considered. According to these values, linear and trigonometric recovery models result in approximately the same resilience of the bridge, whereas the negative exponential recovery function results in very high resilience of the test-bed bridge even if the bridge experienced severe damage. This is because of the exponential nature of this recovery function that indicates a very quick post-disaster recovery of a system resulting in minimal loss even for a severe damage condition. In reality, the rate of initial recovery is not extremely fast as an exponential function because of postevent reconnaissance, damage assessment, and planning to initiate rehabilitation before which the recovery process cannot be started. Hence, a negative exponential recovery model for all bridge damage states is far from reality and not applicable for most of the real-life disaster scenarios. Zhou *et al*. [22] proposed a linear recovery function on the basis of experience gained from bridge recovery during past earthquakes. Therefore, the present study uses linear recovery function for the rest part of this paper.

5. BRIDGE SEISMIC RETROFIT AND ENHANCEMENT IN RESILIENCE

To calculate the effectiveness of bridge retrofit in enhancing seismic resilience, retrofit strategies are applied considering the pre-Northridge undamaged condition of the bridge. The as-built bridge failed in shear. Hence, bridge retrofit techniques that can facilitate the reduction of shear demand in bridge piers should be selected. After exploring various seismic retrofit possibilities for the test-bed bridge, it is found that the application of steel jackets around bridge piers in bents 6, 7, and 8 is the most effective technique for the current purpose [37]. Seismic vulnerability and resilience of the retrofitted bridge are discussed in this section.

5.1. Moment–rotation behavior of retrofitted bridge piers

Steel jackets have been used as a retrofit measure to enhance the flexural ductility and shear strength of reinforced concrete bridge piers. These are typically steel casings that are applied to bridge piers keeping a space of about 50.8 mm at pier ends to prevent the jacket from bearing on adjacent members. Full length of bridge piers in bents 6, 7, and 8 are jacketed with 0.4 mm thick steel jackets. The jacket thickness is decided on the basis of practical consideration of handling the jacket

DOI: 10.1002/eqe

during retrofit operation. Due to jacketing, moment–rotation behaviors of retrofitted piers are improved (shown in Figure 6) that resulted in enhanced rotational ductility of bridge piers.

5.2. *Bridge vulnerability and seismic resilience*

Flexural capacity of piers increased significantly after retrofit with steel jackets (Figure 6). Shear capacity of these piers is estimated following FHWA recommendations [38]. To develop seismic vulnerability model of the retrofitted bridge, time history analysis of the bridge is performed under the same set of 60 ground motions. It is observed that among 60 cases, only for eight cases the bridge had minor damage due to flexure. No higher flexural damage (such as moderate, major, and complete collapse) is observed because bridge excitation under 60 ground motions. Also, no shear damage is observed in any of the retrofitted bridge piers. To confirm the observation, another method proposed by Sakino and Sun [39] to calculate shear capacity of jacketed concrete bridge piers is used, and high values of shear capacity of bridge piers are obtained [37]. Based on this damage scenario, fragility curve of the retrofitted bridge is developed only at the minor damage state (Figure 7). The median value of the fragility curve is estimated to be 1.27 g with a log-standard deviation of 0.5.

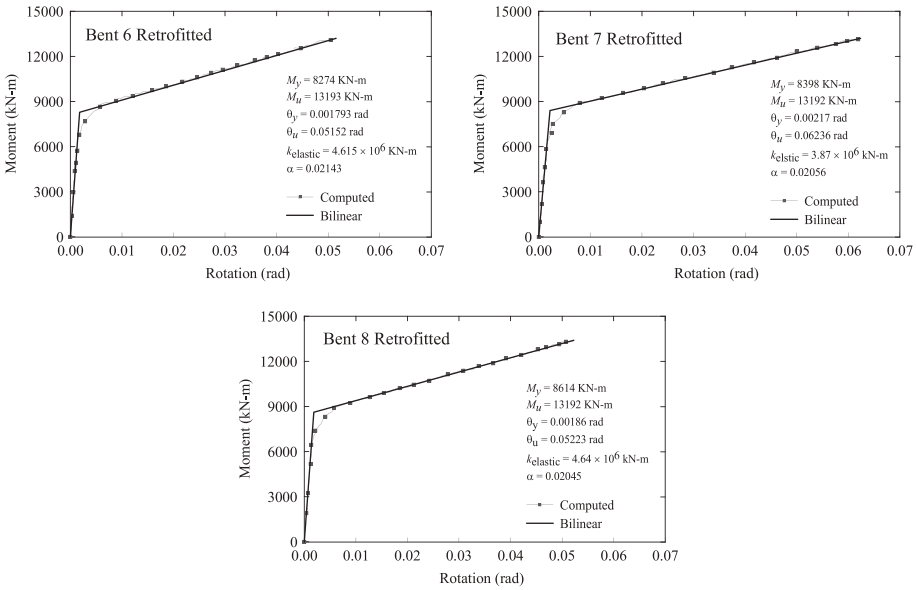

Figure 6. Moment–rotation diagrams of retrofitted piers in bents 6, 7, and 8.

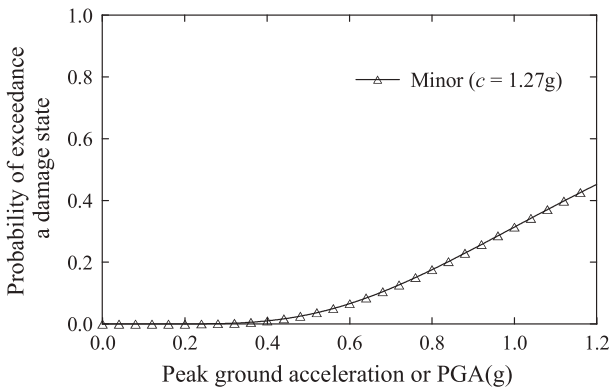

Figure 7. Fragility curves at minor damage state of the retrofitted bridge.

DOI: 10.1002/eqe

Due to the strong seismic fragility characteristics of the retrofitted bridge, an overall loss ratio of 0.09 is calculated for this bridge under the Northridge earthquake. A linear recovery function with an appropriate model for recovery time is considered to calculate seismic resilience. Result shows 99.97% resilience of the bridge under the Northridge earthquake if the bridge were retrofitted with steel jacket prior to the event. Hence, a 74% increase in seismic resilience of the bridge is observed because of seismic retrofitting.

6. SENSITIVITY STUDY AND UNCERTAINTY ANALYSIS

It is recognized that the uncertainties involved with various parameters in the resilience calculation module may introduce uncertainty in the calculated resilience. A sensitivity study is performed to analyze the impact of various uncertain parameters on seismic resilience. For this, the Northridge earthquake is considered as the scenario event for which bridge resilience is estimated. As retrofitting resulted in very high resilience under this scenario event, it would not be possible to distinguish any positive impact of uncertain parameters on seismic resilience if the sensitivity study is performed on the retrofitted bridge. Thus, the un-retrofitted (original) bridge is used for the sensitivity analysis. Although the original bridge is too vulnerable under the Northridge earthquake, estimated resilience of the bridge is 57.47% when a linear recovery function is used. This value is the most expected value of resilience when mean values of all input parameters are considered. Due to uncertainty in input parameters, a distribution of resilience will be observed on both sides of the most expected value of resilience. Note that the observation made from this sensitivity study will be restricted to the case study performed here and may not be applicable to any bridge and seismic event in general.

6.1. Uncertain parameters

The study considers recovery time, control time, indirect to direct loss ratio, and bridge fragility parameters (median values) to be the uncertain parameters. These parameters are statistically independent. Other parameters in the analysis module are considered to be deterministic, and their values are kept fixed. For sensitivity study, each uncertain parameter is varied individually while keeping all other parameters at their respective mean values. A linear recovery function is used to calculate resilience for each case.

(1) Recovery time: To observe the sensitivity of seismic resilience to recovery time, T_{RE} at different bridge damage states are considered to have normal distributions (Table I). The as-built bridge had shear failure during the Northridge earthquake. Consequently, a normal distribution with a mean value of 75 days and standard deviation of 42 days is used to model the uncertainty of recovery function for the as-built bridge. Seismic resilience of the bridge is calculated for mean ± standard deviation of the recovery time.
(2) Control time: In general, the control time T_{LC} is decided by engineers or bridge owners. It depends on the time window of interest, and thus, it can be higher or less than the recovery time. The resilience of the as-built bridge is calculated for mean ± standard deviation of the control time to calculate its influence on bridge resilience. In the present study, the control time is assumed to have a normal distribution with a mean value and standard deviation of 85 days and 40 days, respectively.
(3) Indirect to direct loss ratio: The indirect to direct loss ratio may vary between 5 and 20 [25]. Even higher variation can be observed on the basis of important physical and decision-making parameters including system redundancy, population type and density, preparedness for postevent recovery, and fund allocation. The present study considers the most expected value of indirect to direct loss ratio to be 13 with a standard deviation of 8. With this, the entire range of indirect to direct loss ratio as stated in [25] is covered.
(4) Fragility parameters: Fragility parameters of the bridge may vary because of uncertainty of parameters pertaining to the structure and ground motions. A detail uncertainty analysis considering all uncertain bridge and ground motion parameters is beyond the scope of the present study. For this reason, variability (or uncertainty) of fragility curves is quantified in terms of 90%

DOI: 10.1002/eqe

confidence intervals (between 5% and 95% confidence levels) of these curves. This is a reasonable approach to model the uncertainty associated with fragility curves in absence of any detail uncertainty quantification analysis. Fragility parameters at 95% and 5% confidence levels (with 95% and 5% exceedance probabilities, respectively) are estimated following the procedure described in previous studies [20, 40]. Fragility parameters with 95%, 50%, and 5% confidence bands are listed given in Table V.

6.2. *Methods for sensitivity analysis*

The FOSM reliability analysis is performed for this sensitivity study. In this, the resilience of the as-built bridge is considered to be the performance function. The value of resilience is calculated for mean ± standard deviation of each uncertain parameter. When one parameter is varied, values of other uncertain parameters are kept at their respective mean values. The analysis provides relative variances that can be defined as the ratio of variance of resilience due to i^{th} random variable to the total variance of resilience due to all random variables [41]. In other words, relative variance represents the relative contribution of each uncertain parameter to the total uncertainty of resilience. Hence, values of relative variance indicate the influence of each random variable on the performance function. Figure 8 shows the relative variance for each uncertain parameter. As the figure shows, the recovery time T_{RE} and control time T_{LC} have the major influence on seismic resilience of the bridge. Uncertainties in indirect to direct loss ratio and bridge fragility have no influence on resilience.

A tornado diagram, shown in Figure 9, is also developed to represent the hierarchy of uncertain parameters for seismic resilience of the bridge [23]. The center dotted line in the diagram represents the most expected value of resilience (equal to 57.47%) when mean values of all uncertain parameters are considered. Swings of resilience on both sides of the dotted line show variations of seismic resilience for mean ± standard deviation values of each uncertain parameter. The longer the swing, the higher the influence of the corresponding input parameter on the output. Again, each parameter is varied independently keeping all other parameters at their respective mean values. This

Table V. Fragility parameters with 90% confidence intervals.

	Median fragility parameter (g)		
Damage state	95% confidence	50% confidence	5% confidence
Minor	0.101	0.115	0.130
Moderate	0.197	0.214	0.234
Major	0.356	0.382	0.407
Collapse	0.389	0.414	0.441

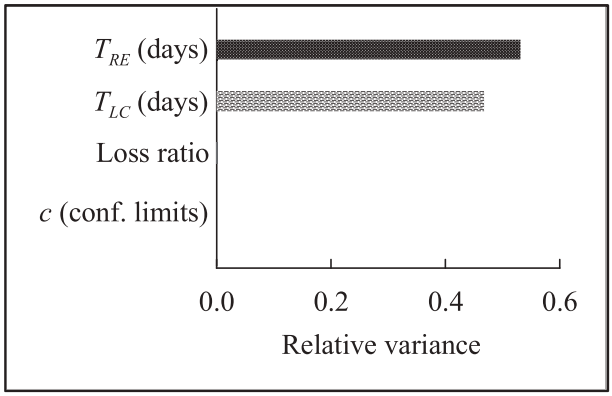

Figure 8. Relative variance of uncertain parameters.

DOI: 10.1002/eqe

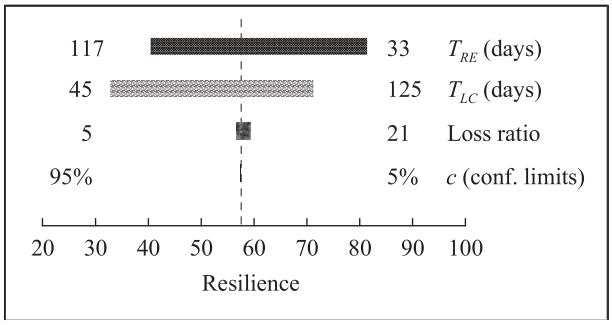

Figure 9. Tornado diagram with uncertain parameters.

tornado diagram shows the same hierarchy as seen from FOSM, and hence confirms the sensitivity of seismic resilience on recovery time and control time.

6.3. *Uncertainty of seismic resilience*

It is evident from Figure 9 that seismic resilience is directly proportional to T_{LC} and inversely proportional to T_{RE}. Figure 10 shows independent influences of T_{RE} and T_{LC} on the variation of seismic resilience R. In this figure, the variation of R with T_{LC} is obtained when T_{RE} is kept at its mean value (=75 days). Similarly, T_{LC} is set to its mean value (=85 days) when the variation of R with T_{RE} is obtained. As the figure shows, resilience varies linearly with T_{RE} and T_{LC} until $T_{RE} = T_{LC}$ (points A and B on the figure). Beyond this, resilience has nonlinear variations with these parameters. The linear trend is obvious as a linear recovery function is used to evaluate resilience for the sensitivity study. The value of resilience will eventually reaches to an asymptotic value if T_{LC} and T_{RE} are increased further beyond their maximum values shown in the figure.

To observe the uncertainty in seismic resilience of the bridge under the Northridge earthquake, Latin Hypercube random sampling technique [42] is used to generate random combinations of T_{RE} and T_{LC}. The advantage of this sampling technique is the randomness in data selection such that not a single data is repeated to form combinations. Normal distributions of T_{RE} and T_{LC} as discussed in Section 6.1 are used for random sampling. Range of each random variable is divided into four equally probable intervals that resulted into 24 random combinations of T_{RE} and T_{LC}. For each combination, seismic resilience is estimated, which is observed to have a wide range variation from 17% to 99%. To estimate the uncertainty associated with these resilience values, a suitable random distribution is assigned to describe the statistical nature of seismic resilience. A goodness-of-fit test revealed that a normal distribution cannot be rejected at significance levels of 0.10 and 0.20 to define seismic resilience. The mean, standard deviation, and coefficient of variation of the normal distribution are 53.73%, 23.98%, and 45%, respectively. This high uncertainty in seismic resilience is the result of high variations considered in

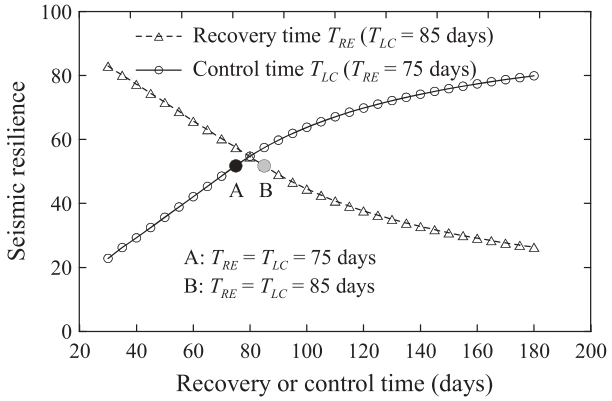

Figure 10. Variation of resilience with recovery time T_{RE} and control time T_{LC}.

DOI: 10.1002/eqe

recovery and control times. The distribution is further verified by plotting resilience values in a normal probability paper (Figure 11(a)). Figure 11(b) shows the cumulative distribution function (CDF) of the normal distribution and 24 values of resilience generated through random sampling of T_{RE} and T_{LC}. As the figure shows, the generated 24 values of resilience cover 92% probability (between 4th and 96th percentile values) that is nearly equal to the mean ±2 times standard deviation of the normal CDF.

Note that the quantification of uncertainty of seismic resilience due to uncertain T_{RE} and T_{LC} is the focus of this section. It is realized that very low value of T_{LC} compared to T_{RE} may not be practically possible, and hence all values of resilience as obtained through the random sampling of T_{RE} and T_{LC} may not be realistic to the test-bed bridge. However, all combinations of T_{RE} and T_{LC} are considered in the study for the completeness of uncertainty analysis. Furthermore, the nature of obtained distribution of resilience and distribution parameters may change if different distributions of T_{RE} and T_{LC} are considered. Hence, the quantified uncertainty in seismic resilience may not be generally applicable to any bridge and damage scenario.

7. COST-BENEFIT ANALYSIS

Through the calculation of seismic resilience, this study showed that the failure and associated losses of the as-built bridge could have been avoided if the bridge piers were retrofitted with steel jackets prior to the Northridge event. In this relation, it is also important to justify the cost associated with seismic retrofitting. A cost-benefit analysis is performed here in which cost of retrofit and benefit from retrofit is calculated. If calculated benefit is more than cost of retrofit, the retrofit strategy is regarded to be cost-effective.

7.1. Cost of retrofit

The cost of retrofitting three bridge piers in bents 6, 7, and 8 using steel jacket is determined using the information of the California Department of Transportation (Caltrans) contract cost database. The cost for such a bridge retrofit type is calculated on the basis of the weight (in lb) of concrete of the element that is to be jacketed. From historic bid data, unit cost price for retrofit with steel jacket is found to be \$2/lb. With this, total cost of retrofit of three bridge piers is calculated to be equal to \$168,800.

7.2. Benefit from retrofit

Bridge retrofit helps in reducing bridge damage and costs because of direct and indirect losses after a seismic event. The expected reduction in loss is considered to be the benefit from seismic retrofit. Thus, the annual benefit $\overline{B}$ due to seismic retrofit can be expressed as [22]

$$\overline{B} = \sum_{m=1}^{M} \left[\left(C_{dm}^{0} - C_{dm}^{R} \right) + \left(C_{im}^{0} - C_{im}^{R} \right) \right] p_m \tag{6}$$

where C_{dm}^{0} and C_{im}^{0}, respectively, are the direct and indirect losses arise from the non-retrofitted bridge due to earthquake m, while C_{dm}^{R} and C_{im}^{R} represent the same quantities from the retrofitted bridge.

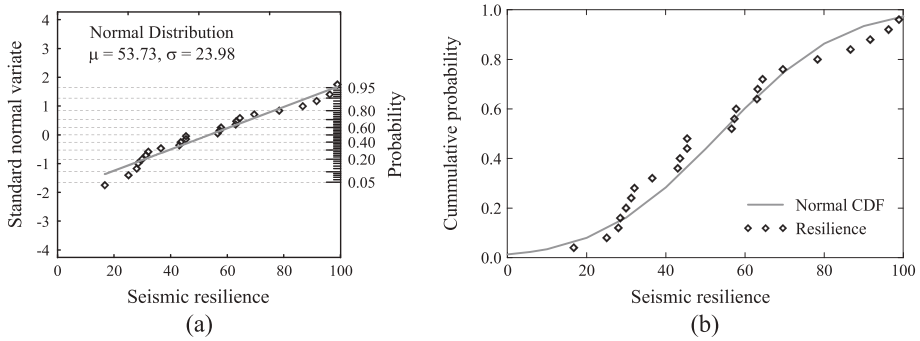

Figure 11. Uncertainty in seismic resilience of the bridge estimated for the Northridge earthquake: (a) normal probability paper and (b) normal CDF.

DOI: 10.1002/eqe

M represents regional scenario earthquakes that the bridge may experience during its service life, and p_m is the annual occurrence probability of these scenario events.

The area of Los Angeles has several active seismic faults that are capable in producing hundreds of earthquakes in the future. For seismic risk assessment, Chang *et al*. [43] performed probabilistic seismic hazard analysis and developed a set of 47 scenario earthquakes that realistically represent the seismic hazard of the Los Angeles region. These 47 scenario earthquakes are used here to calculate benefit from bridge retrofit. To predict possible damage of the bridge (before and after retrofit) due to these scenario seismic events, PGAs of these events at the bridge site are estimated using attenuation relation given by Abrahamson and Silva [44]. These PGA values are used to predict probabilities of bridge damage at various damage states with the use of fragility curves. Calculated probabilities of bridge damage are further used to compute direct and indirect losses before and after bridge retrofit and put into Equation (6) to calculate annual benefit. Thus, the difference in cost as calculated from Equation (6) is the cost avoidance due to seismic retrofit and expressed here as an annual benefit from retrofit.

The annual benefit from retrofit cumulates over the service life of the bridge. Assuming that the design service life of the test-bed bridge was taken to be equal to 75 years when it was designed in 1964 and the retrofit was applied in 1994 prior to the Northridge event, the retrofitted bridge could serve at least another 45 years. Over this remaining service life of the bridge, total benefit B is calculated using a uniform series [22] as given in the following equation.

$$B = \overline{B}\frac{(1+v)^T - 1}{v(1+v)^T} \tag{7}$$

Here, $\overline{B}$ the annual benefit of the seismic retrofit as obtained from Equation (6), v is the discount rate, and T is the remaining service life of the bridge after retrofit. For analytical purpose, T is varied between 30 to 50 years. The total benefit from bridge retrofit is calculated using two discount rates of 3% and 5%.

7.3. Benefit-cost ratio

The total benefit is divided by cost of retrofit to calculate benefit-cost ratio. Table VI represents benefit-cost ratios of seismic retrofit. As can be seen, the benefit-cost ratio is more than one for all cases considered here, which indicates that the retrofit is cost-effective in general. A higher bridge service life results in more cost-effectiveness, whereas the higher discount rate yields less cost-effectiveness of bridge seismic retrofit.

8. CONCLUSIONS

Seismic resilience of a multispan reinforced concrete highway bridge is estimated in the present study. The bridge experienced severe damage during the 1994 Northridge earthquake due to shear failure of one bridge pier in the transverse direction of the bridge. The present study developed the seismic vulnerability model of the bridge in the form of fragility curves at different bridge damage states. These curves provide 100%, 99.7%, 95.3%, and 93.5% failure probabilities of the bridge, respectively, in the minor, moderate, major damage, and complete collapse states due to lateral

Table VI. Summary of benefit-cost ratio.

	Service life (years), T		
Discount rate (v)	30	40	50
3%	1.82	2.14	2.38
5%	1.42	1.59	1.69

DOI: 10.1002/eqe

shaking induced by the horizontal ground motion component of the Northridge earthquake. These failure probability values also predict bridge damage at higher damage states under the Northridge earthquake. From these failure probabilities, direct and indirect losses due to bridge damage are calculated. Seismic resilience of the bridge is evaluated by combining seismic vulnerably and loss models with a suitable post-earthquake recovery model considered for the bridge. The study explored three different recovery models and observed that the linear recovery model that resulted in 57.47% seismic resilience of the bridge is the most suitable model for the current purpose.

Effect of bridge seismic retrofit on seismic resilience is investigated through the application of steel jackets to three bridge piers assuming that the retrofit is applied prior to the Northridge event. It is observed that the seismic performance of the bridge enhanced significantly after bridge retrofit, resulting in 74% increase in seismic resilience of the retrofitted bridge. A benefit-cost analysis showed that the applied retrofit strategy would be cost-effectiveness if the retrofitted bridge can be serviceable for 30 to 50 years post retrofit.

Sensitivity study through the FOSM reliability and tornado diagram analyses revealed that the recovery time and control time are the two most important parameters to which the seismic resilience of the original bridge calculated for the Northridge earthquake is most sensitive. It is also observed from the same analyses that uncertainties in indirect to direct loss ratio and bridge fragility parameters have negligible impact on estimated seismic resilience. For the same case study, uncertainty analysis with random sampling of recovery and control times exhibited that the probabilistic nature of seismic resilience can be described with a normal distribution having 45% coefficient of variation. This high uncertainty in seismic resilience is a result of high variations considered in recovery and control times.

It should be noted that the identified most sensitive parameters and estimated uncertainty in seismic resilience is specific to the case study performed here and uncertainties considered in input parameters. More general conclusions can be drawn through the analysis of a higher population of highway bridges under a variety of seismic motions.

ACKNOWLEDGEMENTS

The research is partially supported by the Mid-Atlantic Universities Transportation Center (MAUTC) of the University Transportation Centers Program through project PSU-2012-01.

REFERENCES

1. Caltrans seismic retrofit program. Available from: http://www.dot.ca.gov/hq/paffairs/about/retrofit.htm [February 14, 2011].
2. WSDOT Washington State's bridge seismic retrofit program. http://www.wsdot.wa.gov/eesc/bridge/preservation/pdf%5CBrgSeismicPaper.pdf [February 14, 2011].
3. Wright T, DesRoches R, Padgett JE. Bridge seismic retrofitting practices in the central and southeastern United States. *Journal of Bridge Engineering* 2011; **16**(1):82–92.
4. Casciati F, Cimellaro GP, Domaneschi M. Seismic reliability of a cable-stayed bridge retrofitted with hysteretic devices. *Computer and Structures* 2008; **86**:1769–1781.
5. Chang SE, Nojima N. Measuring post-disaster transportation system performance: the 1995 Kobe earthquake in comparative perspective. *Transportation Research Part A: Policy and Practice* 2001; **35**(6):475–494.
6. Bruneau M, Chang S, Eguchi R, Lee G, O'Rourke T, Reinhorn A, Shinozuka M, Tierney K, Wallace W, von Winterfelt D. A framework to quantitatively assess and enhance the seismic resilience of communities. *Earthquake Spectra* 2003; **19**(4):733–752.
7. Chang S, Chamberlin C. Assessing the role of lifeline systems and community disaster resilience. *MCEER Research Progress and Accomplishments* 2004; 2003–04. Buffalo, NY.
8. Shinozuka M, Chang SE, Cheng TC, Feng M, O'Rourke TD, Saadeghvaziri MA, Dong X, Jin X, Wang Y, Shi P. Resilience of integrated power and water systems. *MCEER Research Progress and Accomplishments* 2004; 2003–2004, 65–86. Buffalo, NY.
9. Rose A, Liao SE. Modeling regional economic resiliency to earthquakes: a computable general equilibrium analysis of water service disruptions. *Journal of Regional Science* 2005; **45**:75–112.
10. Paton D, Johnston D. Lifelines and urban resilience. *Disaster Resilience an Integrated Approach*, Chapter 4. Charles C Thomas Publisher LTD., 2006. ISBN 0-398-07663-4 – ISBN 0-398-07664-2
11. Amdal JR, Swigart SL. Resilient transportation systems in a post-disaster environment: a case study of opportunities realized and missed in the greater New Orleans region. *UNOTI Publications*: Paper 5, 2010.
12. Cimellaro GP, Reinhorn AM, Bruneau M. Framework for analytical quantification of disaster resilience. *Engineering Structures* 2010; **32**:3639–3649.

DOI: 10.1002/eqe

13. Arcidiacono V, Cimellaro GP, Reinhorn AM, Bruneau M. Community resilience evaluation including interdependencies. *15th World Conference on Earthquake Engineering* (15WCEE), Lisbon, Portugal, September 24–28th, 2012.
14. Decò A, Bocchini P, Frangopol DM. A probabilistic approach for the prediction of seismic resilience of bridges. *Earthquake Engineering and Structural Dynamics* 2013; **42**(10):1469–1487.
15. Cimellaro GP. Resilience-based design (RBD) modelling of civil infrastructure to assess seismic hazards. *Handbook of Seismic Risk Analysis and Management of Civil Infrastructure Systems*, Tesfamariam S, Canada, Goda K, University of Bristol, UK (eds.), Woodhead Publishing Limited, Cambridge, UK, 2013.
16. DeBlasio AJ, Zamora A, Mottley F, Brodesky F, Zirker ME, Crowder M. Effects of catastrophic events on transportation system management and operations, Northridge earthquake – January 17, 1994. *Technical Report*, U.S. Department of Transportation, Federal Highway Administration, Washington, DC, 2002.
17. Cofer WF, Mclean DI, Zhang Y. Analytical evaluation of retrofit strategies for multi-column bridges. *Technical Report for Washington State Transportation Centre (TRAC)*, Washington State University, Pullman, Washington, 1997.
18. Cimellaro GP, Reinhorn AM, Bruneau M. Seismic resilience of a hospital system. *Structure and Infrastructure Engineering* 2010; **6**(1–2):127–144.
19. Banerjee S, Shinozuka M. Mechanistic quantification of RC bridge damage states under earthquake through fragility analysis. *Probabilistic Engineering Mechanics* 2008; **23**(1):12–22.
20. Banerjee S, Shinozuka M. Experimental verification of bridge seismic damage states quantified by calibrating analytical models with empirical field data. *Journal of Earthquake Engineering and Engineering Vibration* 2008; **7**(4):383–393.
21. Prasad GG, Banerjee S. The impact of flood-induced scour on seismic fragility characteristics of bridges. *Journal of Earthquake Engineering* 2013; **17**(9):803–828.
22. Zhou Y, Banerjee S, Shinozuka M. Socio-economic effect of seismic retrofit of bridges for highway transportation networks: a pilot study. *Structure and Infrastructure Engineering* 2010; **6**(1–2):145–157.
23. Banerjee S, Prasad GG. Seismic risk assessment of reinforced concrete bridges in flood-prone regions. *Structure and Infrastructure Engineering* 2013; **9**(9):952–968.
24. HAZUS. Earthquake loss estimation methodology. *Technical Manual SR2*, Federal Emergency Management Agency through agreements with National Institute of Building Science, Washington, DC, 1999.
25. Dennemann LK. Life-cycle cost benefit (LCC-B) analysis for bridge seismic retrofits. *MS Thesis*, Rice University, TX, 2009.
26. HAZUS–MH MR3. Multi-hazard loss estimation methodology – earthquake model. *Technical Manual*, Department of Homeland Security, Washington, DC, 2003.
27. ATC-13. *Earthquake Damage Evaluation Data for California*. Applied Technology Council: Redwood City, CA, 1985.
28. Broderick BM, Elnashai AS. Analysis of the failure of Interstate 10 Freeway ramp during the Northridge earthquake of 17 January 1994. *Earthquake Engineering and Structural Dynamics* 1994; **24**:189–208.
29. Lee DH, Elnashai AS. Inelastic seismic analysis of RC bridge piers including flexure-shear interaction. *Structural Engineering and Mechanics* 2002; **12**(3):241–260.
30. Computer and Structures, Inc. SAP2000 (Structural Analysis Program), Berkeley, CA, Version 15.0, 2011.
31. Bentley Structures. STAADPro Section Designer, Yorba Linda, CA, 2011.
32. Priestley MJN, Seible F, Calvi GM. *Seismic Design and Retrofit of Bridges*. John Wiley & Sons, Inc.: New York, NY, 1996.
33. Nielson BG, DesRoches R. Influence of modeling assumptions on the seismic response of multi-span simply supported steel girder bridges in moderate seismic zones. *Engineering Structures* 2006; **28**:1083–1092.
34. Caltrans. *Seismic Design Criteria*. California Department of Transportation, Division of Structures: Sacramento, CA, 1999.
35. Pekcan G. Design of seismic energy dissipation systems for concrete and steel structures. *Ph.D. Dissertation*, University at Buffalo, State University of New York, Buffalo, NY, 1998.
36. Shinozuka M, Feng MQ, Kim H, Uzawa T, Ueda T. Statistical analysis of fragility curves. *Technical Report*, Multidisciplinary Center for Earthquake Engineering Research, State University at Buffalo, Buffalo, NY, 2000.
37. Venkittaraman A. Seismic resilience of highway bridges. *MS Thesis*, The Pennsylvania State University, University Park, PA, 2013.
38. FHWA. Seismic retrofitting manual for highway structures: part 1 – bridges, Federal Highway Management Agency, Publication No. FHWA-HRT-06-032, 2006.
39. Sakino K, Sun Y. Steel jacketing for improvement of column strength and ductility. *12th World Conference on Earthquake Engineering*, Auckland, January 30 – February 4, New Zealand, 2000.
40. Banerjee S, Shinozuka M, Sgaravato M. Uncertainty in seismic performance of highway network estimated using empirical fragility curves of bridges. *International Journal of Engineering under Uncertainty: Hazard, Assessment, and Mitigation* 2009; **1**(1–2):1–11.
41. Ang A, Tang W. *Probability Concepts in Engineering Planning and Design: Decision, Risk, and Reliability*. John Wiley & Sons: New York, 1984.
42. McKay MD. Latin hypercube sampling as a tool in uncertainty analysis of computer models. *Proceedings of the 24th Winter Simulation Conference*, Virginia, 1992; 557–564.
43. Chang ES, Shinozuka M, Moore J. Probabilistic earthquake scenarios: extending risk analysis methodologies to spatially distributed systems. *Earthquake Spectra* 2000; **16**(3):557–572.
44. Abrahamson N, Silva W. Summary of the Abrahamson & Silva NGA ground motion relations. *Earthquake Spectra* 2008; **24**(1):67–97.

DOI: 10.1002/eqe